LTE Fingerprinting Localization with Altitude

Torbjörn Wigren, *Senior Member, IEEE*

Ericsson AB, SE-16480, Stockholm, SWEDEN. torbjorn.wigren@ericsson.com

***Abstract*—The paper shows how to add altitude to the adaptive enhanced cell identity (AECID) fingerprinting localization method in the long term evolution (LTE) cellular system. This improves the precision of E-911 emergency positioning in vertically extended regions like in tall buildings. The altitude is added to the corners of a polygon using assisted GPS (A-GPS), observed time difference of arrival (OTDOA) or uplink time difference of arrival (U-TDOA) altitude measurements of opportunity. A new algorithm transforms to a 3-dimensional point with an ellipsoidal uncertainty, since the latter format is standardized on all LTE position reporting interfaces.**

I. INTRODUCTION

The main localization technology to be deployed for E-911 emergency positioning [1] in the LTE cellular system is expected to be A-GPS [2]-[4]. Most smart phones are equipped with A-GPS receiver hardware today, and the penetration is increasing. However, even with fine time assistance, A-GPS has limited indoor and urban canyon coverage [2], [4]. Therefore the LTE standard includes a high precision terrestrial OTDOA positioning method [2]. A corresponding U-TDOA method is also being standardized [2], [5]. The terrestrial methods are not as accurate as A-GPS though, and they rely on a base station deployment with good geometrical properties. This can be prohibitive in rural areas [6]. Furthermore, the latencies of A-GPS, OTDOA and U-TDOA make them less suitable for certain lower precision location based services. Hence, there is a need for fallback like cell identity (CID) positioning [2], combined with timing advance (TA) [2], [7] and angle of arrival (AoA) [2], [8] information.

The LTE positioning protocol (LPP) [9] and the LTE positioning protocol annex (LPPa) [10] are also fully prepared to carry fingerprinting information [2]. The fingerprinting information may contain CIDs and received signal strengths (RSSs) from the serving and neighbor cells, TA of the serving cell, as well as AoA information. Fingerprinting positioning exploits detailed geographical maps of radio signatures [2]. The radio signature maps are generated by predication software (SW), surveying [11], or by a combination. To perform a positioning, the radio signature is measured by the terminal and the location that fits the measured radio signature the best is looked up and selected as the estimated position. Enhancements to radio signature mapping for the global system for mobile communication (GSM) is discussed in [12]. Further fingerprinting implementation in GSM is reported in [11], [13] and [14], where [11] and [13] focus on received signal strength and where [14] treats the use of TA.

Unfortunately, surveying becomes a formidable task for a nationwide cellular network. Secondly, also radio propagation prediction SW requires much work with 3-dimensional (3D) geographical modeling with building resolution. Thirdly, neither surveying nor the use of SW can capture effects of varying (handheld) cellular terminal orientation. These variations result in antenna gain variations exceeding 10 dBs, giving positioning uncertainties approaching 50% of the cell radius [5], [14]. The adaptive enhanced cell identity (AECID) positioning method [6], [15] addresses the above drawbacks by the measurement of fingerprinting information, *whenever* high precision A-GPS, OTDOA or U-TDOA position measurements occur in the LTE network. The high precision measurements with the same fingerprint are then clustered [16] and a 3GPP polygon [17] that describes the boundary of the cluster is computed. Cellular terminal orientation is then automatically captured in the radio map generation. The availability of OTDOA and U-TDOA in LTE secures indoor coverage of the radio maps.

The scope of the paper is to extend the AECID method to provide 3-dimensional (3D) positioning. The first technical contribution uses altitude information from A-GPS, OTDOA and U-TDOA positions of opportunity to provide the AECID radio map with fingerprinted polygons with altitude. This geographical format is not a part of the reporting standards of [9] and [10]. To be able to report the 3D-position, the second contribution derives a geographical shape conversion algorithm from the polygon with altitude, to the 3GPP ellipsoid point with altitude and uncertainty ellipsoid of [17].

The paper summarizes the AECID algorithm in section II. Section III treats 3D radio maps, while section IV concentrates on the new shape conversion. The methods are illustrated numerically in section V. Conclusions follow in section VI.

II. 2-DIMENSIONAL AECID POLYGON COMPUTATION

The starting point consists of A-GPS, OTDOA or U-TDOA positions of opportunity (superscript ^{m}), fingerprinted and available in the cluster with fingerprint $^{\mathbf{p}}$ as

$$\mathbf{r}_j^{m,\mathbf{p}} = \left(x_j^{m,\mathbf{p}} \quad y_j^{m,\mathbf{p}} \quad z_j^{m,\mathbf{p}}\right)^T, \quad j = 1,...,J^{\mathbf{p}}. \tag{1}$$

It is assumed that $\mathbf{r}_j^{m,\mathbf{p}}$ are given in a Cartesian East-North-Up (ENU) earth-tangential coordinate system, see e.g. [2], [4].

A. Polygon Initialization

The first step is to compute a *contraction point* for a 2-dimensional (2D) polygon, disregarding $z_j^{m,\mathbf{p}}$ of (1). Following [6], the 2D center of gravity of the points of (1) is

$$\mathbf{r}_{CG}^{\mathbf{p}2D} = \left(x_{CG}^{\mathbf{p}2D} \quad y_{CG}^{\mathbf{p}2D}\right)^T = \frac{1}{J^{\mathbf{p}}}\sum_{j=1}^{J^{\mathbf{p}}}\left(x_j^{m,\mathbf{p}} \quad y_j^{m,\mathbf{p}}\right)^T. \tag{2}$$

978-1-4673-1881-5/12/$31.00 ©2012 IEEE

The distances between the points of the cluster and (2) are then computed and sorted. A selected fraction of the points of the cluster, that are closest to the global center of gravity are extracted. This results in a set of closest reference points

$$\left\{\left(x_{j_{local}}^{m,\mathbf{p}} \quad y_{j_{local}}^{m,\mathbf{p}}\right)^T\right\}_{j_{local}=1}^{J_{local}^{\mathbf{p}}}, \tag{3}$$

where $J_{local}^{\mathbf{p}}$ denotes the number of reference points in the set. The local center of gravity then follows as

$$\mathbf{r}_{CG,local}^{\mathbf{p},2D} = \left(x_{CG,locaal}^{\mathbf{p},2D} \quad y_{CG,local}^{\mathbf{p},2D}\right)^T = \frac{1}{J_{local}^{\mathbf{p}}}\sum_{j_{local}=1}^{J_{local}^{\mathbf{p}}}\left(x_{j_{local}}^{m,\mathbf{p}} \quad y_{j_{local}}^{m,\mathbf{p}}\right)^T \tag{4}$$

The use of a local center of gravity ensures that the contraction point is in the interior of the cluster, even if the cluster is narrow in the radial direction, wide in the lateral direction and highly curved. The polygon to be computed is then initialized, so that the entire cluster is in the interior of the polygon [15].

B. Polygon Contraction

The polygon is computed with the algorithm of [6], [15]. At each iteration the polygon corners are tested for inward movement towards (4), until exactly one cluster point that was previously in the interior of the polygon, becomes exterior.

The geometry for the tentative movement of Fig. 1 shows the polygon corners $\mathbf{r}_k^{\mathbf{p},2D} = \left(x_k^{\mathbf{p}} \quad \mathbf{y}_k^{\mathbf{p}}\right)^T$, $\mathbf{r}_i^{\mathbf{p},2D} = \left(x_i^{\mathbf{p}} \quad y_i^{\mathbf{p}}\right)^T$ and $\mathbf{r}_l^{\mathbf{p},2D} = \left(x_l^{\mathbf{p}} \quad y_l^{\mathbf{p}}\right)^T$. The middle point $\mathbf{r}_i^{\mathbf{p},2D}$ is then moved towards $\mathbf{r}_{CG,local}^{\mathbf{p}2D}$, leading to movement of the line segments that connect $\mathbf{r}_k^{\mathbf{p},2D}$ and $\mathbf{r}_i^{\mathbf{p},2D}$, and $\mathbf{r}_i^{\mathbf{p},2D}$ and $\mathbf{r}_l^{\mathbf{p},2D}$. To determine a tentative point of intersection with the arbitrary high precision position $\mathbf{r}_j^{m,\mathbf{p},2D}$ of the cluster, the movement

$$\mathbf{r}_i^{\mathbf{p},2D}\left(\alpha^{\mathbf{p}}\right) = \mathbf{r}_i^{\mathbf{p},2D} + \alpha^{\mathbf{p}}\left(\mathbf{r}_{CG,local}^{\mathbf{p},2D} - \mathbf{r}_i^{\mathbf{p},2D}\right), \quad \alpha^{\mathbf{p}} \geq 0, \tag{5}$$

is considered. An intersection requires that $\mathbf{r}_i^{\mathbf{p},2D}\left(\alpha^{\mathbf{p}}\right) - \mathbf{r}_k^{\mathbf{p},2D}$ and $\mathbf{r}_j^{m,\mathbf{p},2D} - \mathbf{r}_k^{\mathbf{p},2D}$ become parallel, or that $\mathbf{r}_i^{\mathbf{p},2D}\left(\alpha^{\mathbf{p}}\right) - \mathbf{r}_l^{\mathbf{p},2D}$ and $\mathbf{r}_j^{m,\mathbf{p},2D} - \mathbf{r}_l^{\mathbf{p},2D}$ become parallel, i.e. that the cross product between the vectors is zero, which gives

$$\alpha_{ik}^{j,\mathbf{p}} = \frac{-\left(x_i^{\mathbf{p}} - x_k^{\mathbf{p}}\right)\left(y_j^{m,\mathbf{p}} - y_k^{\mathbf{p}}\right) + \left(x_j^{m,\mathbf{p}} - x_k^{\mathbf{p}}\right)\left(y_i^{\mathbf{p}} - y_k^{\mathbf{p}}\right)}{\left(x_{CG,local}^{\mathbf{p},2D} - x_i^{\mathbf{p}}\right)\left(y_j^{m,\mathbf{p}} - y_k^{\mathbf{p}}\right) - \left(x_j^{m,\mathbf{p}} - x_k^{\mathbf{p}}\right)\left(y_{CG,local}^{\mathbf{p},2D} - y_i^{\mathbf{p}}\right)} \tag{6}$$

$$\alpha_{il}^{j,\mathbf{p}} = \frac{-\left(x_i^{\mathbf{p}} - x_l^{\mathbf{p}}\right)\left(y_j^{m,\mathbf{p}} - y_l^{\mathbf{p}}\right) + \left(x_j^{m,\mathbf{p}} - x_l^{\mathbf{p}}\right)\left(y_i^{\mathbf{p}} - y_l^{\mathbf{p}}\right)}{\left(x_{CG,local}^{\mathbf{p},2D} - x_i^{\mathbf{p}}\right)\left(y_j^{m,\mathbf{p}} - y_l^{\mathbf{p}}\right) - \left(x_j^{m,\mathbf{p}} - x_l^{\mathbf{p}}\right)\left(y_{CG,local}^{\mathbf{p},2D} - y_i^{\mathbf{p}}\right)}. \tag{7}$$

The subscripts indicate the polygon corner points that define the line segment under evaluation. The superscript denotes the index of the high precision measurement point. A requirement for (6) and (7) to be a valid constraints is that $\alpha_{ik}^{j,\mathbf{p}} > 0$ and $\alpha_{il}^{j,\mathbf{p}} > 0$. It must also be checked if the intersection point falls between the points that limit the line segment of the polygon. i.e. that $\beta_{ik}^{j,\mathbf{p}} \in [0,1]$ or $\beta_{il}^{j,\mathbf{p}} \in [0,1]$, where

$$\mathbf{r}_j^{m,\mathbf{p},2D} = \mathbf{r}_i^{\mathbf{p},2D}\left(\alpha_{ik}^{j,\mathbf{p}}\right) + \beta_{ik}^{j,\mathbf{p}}\left(\mathbf{r}_k^{\mathbf{p},2D} - \mathbf{r}_i^{\mathbf{p},2D}\right) \tag{8}$$

$$\mathbf{r}_j^{m,\mathbf{p},2D} = \mathbf{r}_i^{\mathbf{p},2D}\left(\alpha_{il}^{j,\mathbf{p}}\right) + \beta_{il}^{j,\mathbf{p}}\left(\mathbf{r}_l^{\mathbf{p},2D} - \mathbf{r}_i^{\mathbf{p},2D}\right). \tag{9}$$

The complete evaluation of the intersection with $\mathbf{r}_j^{m,\mathbf{p},2D}$, $j = 1,\ldots,J^{\mathbf{p}}$, performed for all tentative inward movements checks for simultaneous fulfillment of the conditions on $\alpha_{ik}^{j,\mathbf{p}}$, $\alpha_{il}^{j,\mathbf{p}}$, $\beta_{ik}^{j,\mathbf{p}}$, and $\beta_{il}^{j,\mathbf{p}}$.

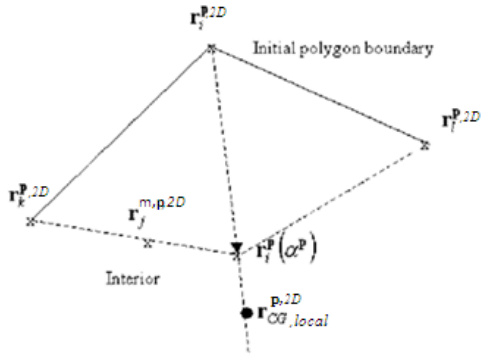

Fig. 1. The geometry of the polygon corner movement.

It also needs to be checked if the inward movement leads to the polygon intersecting itself. Such an intersection between (5), and the line segment between $\mathbf{r}_m^{\mathbf{p},2D}$ and $\mathbf{r}_n^{\mathbf{p},2D}$, is given by

$$\mathbf{r}_i^{\mathbf{p},2D} + \alpha_{i,mn}^{\mathbf{p}}\left(\mathbf{r}_{CG,local}^{\mathbf{p},2D} - \mathbf{r}_i^{\mathbf{p},2D}\right) = \mathbf{r}_m^{\mathbf{p},2D} + \gamma_{mn}^{\mathbf{p}}\left(\mathbf{r}_n^{\mathbf{p},2D} - \mathbf{r}_m^{\mathbf{p},2D}\right), \tag{10}$$

which is solved with respect to the parameters $\alpha_{i,mn}^{\mathbf{p}}$ and $\gamma_{mn}^{\mathbf{p}}$. No solution is computed for corners adjacent to $\mathbf{r}_i^{\mathbf{p},2D}$. Solutions with $\gamma_{mn}^{\mathbf{p}} \notin [0,1]$ are then discarded. The solution with the minimum value of $\alpha_{i,mn}^{\mathbf{p}}$, $\alpha_{i,mn}^{\mathbf{p}} > 0$, $\gamma_{mn}^{\mathbf{p}} \in [0,1]$, is then

$$\alpha_{i,m_0n_0}^{\mathbf{p}}, \gamma_{m_0n_0}^{\mathbf{p}} = \arg\min_{\substack{m,n \\ \gamma_{mn}^{\mathbf{p}} \in [0,1]}} \alpha_{i,mn}^{\mathbf{p}}(m,n). \tag{11}$$

To determine the final tentative inward movement, the smallest value of (6), (7) or (11) is selected.

C. Polygon Corner Selection

A division of the polygon into triangles, followed by integration gives the area reduction caused by movement of $\mathbf{r}_i^{\mathbf{p},2D}$, see [15]. The polygon corner that maximizes the area reduction is then updated, and the limiting cluster point is removed from the list of cluster points that remain in the interior of the contracting polygon.

D. Polygon Re-sampling and Stopping Criterion

The corners of the polygons of laterally wide clusters tend to move laterally. Few points are therefore left for modeling of the outer parts of the geographical region. Reference [6] solves this by a periodic re-distribution of the corners along the momentary polygon boundary, at positions that renders equidistant corners as counted along the boundary.

The 2D polygon computation is stopped when a pre-specified fraction of the cluster points remain in the interior of the polygon, i.e. when the *experimental confidence* has reached the desired level.

III. 3-DIMENSIONAL AECID POLYGON COMPUTATION

With a 2D polygon computed, altitude information of $\mathbf{r}_j^{m,\mathbf{p}}$ can now be used to augment each polygon corner with an altitude. The measured altitude information consists of the altitude and the altitude uncertainty, and it is a part of A-GPS, OTDOA and U-TDOA reports in LTE. The vertical uncertainty is a part of the ellipsoid point with altitude and uncertainty ellipsoid format of [17]. The uncertainty of the altitude measurement is

$$z^{m,\mathbf{p}}_j = z^{m,\mathbf{p}}_{j,0} + \Delta z^{m,\mathbf{p}}_j \tag{12}$$

$$\left(\sigma^{m,\mathbf{p}}_j\right)^2 = \left\langle \left(\Delta z^{m,\mathbf{p}}_j\right)^2 \right\rangle, \tag{13}$$

where $\langle\ \rangle$ denotes the uncertainty estimate performed by the position calculation node of the specific positioning method. The altitude uncertainty estimates vary significantly between the measurements, between terminals, and in particular between A-GPS, OTDOA and U-TDOA. To augment each 2D polygon corner with an altitude, a horizontal search is performed to determine which pre-specified fraction of the total number of points in the cluster, that are closest to each corner. Denoting the closest measurements of the corner i with the subscript $j(i)$, the best linear unbiased estimate (BLUE) for the altitude of each corner is ([18, section 4.3])

$$z^{\mathbf{p}}_i = \left(\sum_{j(i)=1}^{J^{\mathbf{p}}_i} \frac{1}{\left(\sigma^{m,\mathbf{p}}_{j(i)}\right)^2} \right)^{-1} \sum_{j(i)=1}^{J^{\mathbf{p}}_i} \frac{1}{\left(\sigma^{m,\mathbf{p}}_{j(i)}\right)^2} z^{m,\mathbf{p}}_{j(i)} \ . \tag{14}$$

IV. 3D AECID LOCALIZATION AND REPORTING

AECID localization of a terminal in LTE starts with measurement of the fingerprint, followed by a lookup of the AECID 3D polygon. Since the 3GPP reporting standard does not support polygons with altitude, this section derives a transformation of the 3D polygon to a 3GPP standard format, the ellipsoid point with altitude and uncertainty ellipsoid [17].

A. Confidence Model

The confidence is the probability that the terminal is located in the interior of the reported region. The AECID fingerprinting positioning error is caused by radio propagation effects. Hence it is natural to use a uniform statistical model for the terminal location. The ellipsoid that is derived from the 3D polygon must therefore also be associated with a uniform distribution.

B. Uncertainty Ellipsoid

The uncertainty ellipsoid is parameterized with a semi-major axis a, semi-minor axis b and angle φ relative to north, counted clockwise from the semi-major axis. The vertical extension is provided by the vertical uncertainty, c. The confidence is included in the format [17].

C. Horizontal Shape Conversion

The transformation from the 3D polygon to the ellipsoid point with altitude and uncertainty ellipsoid is carried out by a first transformation of the 2D polygon, to a 2D ellipsoid point with an uncertainty ellipse [17]. This part of the transformation determines the horizontal part of the center point of the ellipsoid, and the parameters a, b and φ.

1) Polygon area

The computation of the area is performed by integration between adjacent corners of the polygon, collected in

$$\mathbf{r}^{\mathbf{p},2D} = \left(\mathbf{r}^{\mathbf{p},2D}_1 \quad \ldots \quad \mathbf{r}^{\mathbf{p},2D}_{N^{\mathbf{p}}}\right), \tag{15}$$

where $N^{\mathbf{p}}$ is the number of corners. The area $A^{\mathbf{p},2D}$ is then [19]

$$A^{\mathbf{p},2D} = \frac{1}{2} \sum_{i=1}^{N^{\mathbf{p}}-1} \left(x^{\mathbf{p}}_i y^{\mathbf{p}}_{i+1} - x^{\mathbf{p}}_{i+1} y^{\mathbf{p}}_i \right) + \frac{1}{2} \left(x^{\mathbf{p}}_{N^{\mathbf{p}}} y^{\mathbf{p}}_1 - x^{\mathbf{p}}_1 y^{\mathbf{p}}_{N^{\mathbf{p}}} \right) \tag{16}$$

2) Polygon center of gravity

Standard results, again based on integration [19], gives the center of gravity $\mathbf{r}^{\mathbf{p},2D}_{CG,polygon} = \left(x^{\mathbf{p}}_{CG,polygon} \quad y^{\mathbf{p}}_{CG,polygon}\right)^T$

$$x^{\mathbf{p}}_{CG,polygon} = \frac{1}{6A^{\mathbf{p},2D}} \left(\sum_{i=1}^{N^{\mathbf{p}}-1} \left(x^{\mathbf{p}}_i + x^{\mathbf{p}}_{i+1}\right)\left(x^{\mathbf{p}}_i y^{\mathbf{p}}_{i+1} - x^{\mathbf{p}}_{i+1} y^{\mathbf{p}}_i\right) + \left(x^{\mathbf{p}}_{N^{\mathbf{p}}} + x^{\mathbf{p}}_1\right)\left(x^{\mathbf{p}}_{N^{\mathbf{p}}} y^{\mathbf{p}}_1 - x^{\mathbf{p}}_1 y^{\mathbf{p}}_{N^{\mathbf{p}}}\right) \right) \tag{17}$$

$$y^{\mathbf{p}}_{CG,polygon} = \frac{1}{6A^{\mathbf{p},2D}} \left(\sum_{i=1}^{N^{\mathbf{p}}-1} \left(y^{\mathbf{p}}_i + y^{\mathbf{p}}_{i+1}\right)\left(x^{\mathbf{p}}_i y^{\mathbf{p}}_{i+1} - x^{\mathbf{p}}_{i+1} y^{\mathbf{p}}_i\right) + \left(y^{\mathbf{p}}_{N^{\mathbf{p}}} + y^{\mathbf{p}}_1\right)\left(x^{\mathbf{p}}_{N^{\mathbf{p}}} y^{\mathbf{p}}_1 - x^{\mathbf{p}}_1 y^{\mathbf{p}}_{N^{\mathbf{p}}}\right) \right) \tag{18}$$

3) Polygon orientation

To find the orientation of the ellipsoid, $\pi/2 - \varphi$, a search over lines that pass through the center of gravity of the 2D polygon is performed, to find the line with the longest line segment with end points on the boundary of the polygon. To formulate the algorithmic steps, $\mathbf{r}^{\mathbf{p},2D}_i$ and $\mathbf{r}^{\mathbf{p},2D}_j$ are used to denote two adjacent corners of the polygon. The algorithm is then:

i) Selection of test angles in $[-\pi/2, \pi/2]$.

ii) For each of the lines passing through $\mathbf{r}^{\mathbf{p},2D}_{CG,polygon}$:

   a. Determination of all intersections between the line through $\mathbf{r}^{\mathbf{p},2D}_{CG,polygon}$, and the line segments forming the polygon boundary.

   b. Determination of the longest line segment, defined by the line which passes through $\mathbf{r}^{\mathbf{p},2D}_{CG,polygon}$ and the intersections.

iii) Selection of $\pi/2 - \varphi$ as the angle generating the line segment that is longest, for all angles.

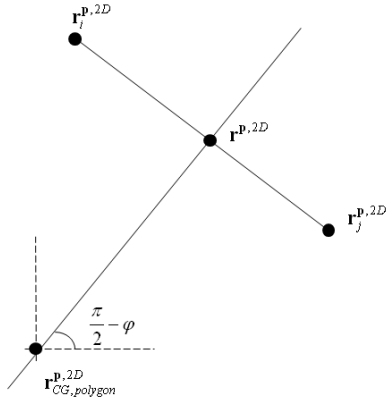

Fig. 2: The geometry for determination of φ.

From Fig. 2, the point $\mathbf{r}^{\mathbf{p},2D}$ on the boundary fulfills

$$\mathbf{r} = \mathbf{r}^{\mathbf{p},2D}_{CG,polygon} + \gamma \begin{pmatrix} \cos(\pi/2 - \varphi) \\ \sin(\pi/2 - \varphi) \end{pmatrix} \tag{19}$$

$$\mathbf{r} = \mathbf{r}^{\mathbf{p},2D}_i + \delta\left(\mathbf{r}^{\mathbf{p},2D}_j - \mathbf{r}^{\mathbf{p},2D}_i\right), \tag{20}$$

Where γ and δ are scalar parameters. The solution to the system of equations defined by (19) and (20) follows as

$$\begin{pmatrix}\gamma\\ \delta\end{pmatrix}=\begin{pmatrix}\cos(\pi/2-\varphi) & x_i^{\mathbf{p}}-x_j^{\mathbf{p}}\\ \sin(\pi/2-\varphi) & y_i^{\mathbf{p}}-x_j^{\mathbf{p}}\end{pmatrix}^{-1}\begin{pmatrix}x_i^{\mathbf{p}}-x_{CG,polygon}^{\mathbf{p}}\\ y_i^{\mathbf{p}}-y_{CG,polygon}^{\mathbf{p}}\end{pmatrix}. \quad (21)$$

For a given φ, and pair of corner points ($\mathbf{r}_i^{\mathbf{p}}$ and $\mathbf{r}_j^{\mathbf{p}}$), the parameters γ and δ are determined. In case $\delta\in[0,1]$, the intersection falls between the corner points and is valid. The calculation of γ and δ are repeated for all line segments of the polygon. Since the direction vector of the line through the center of gravity is normalized, the length of the line segment between the center of gravity and the boundary is given by γ. The intersections k (maximum length) and l (minimum length, other direction) which generate the largest difference

$$l(\pi/2-\varphi)=\gamma_k-\gamma_l, \quad (22)$$

correspond to the sought candidate length for the angle $\pi/2-\varphi$. Finally, the angle that renders the largest value of $l(\pi/2-\varphi)$ is determined, where $_e$ refers to the *ellipse*, i.e.,

$$\pi/2-\varphi_e=\arg\max_{\varphi} l(\pi/2-\varphi)\cdot \quad (23)$$

4) Polygon translation and rotation

The polygon corners are then translated so that the center of gravity of the polygon is moved to the origin. The corners are then rotated so that the orientation coincides with the x-axis:

$$\mathbf{r}^{\mathbf{p},2D'}=\mathbf{r}^{\mathbf{p},2D}-\mathbf{r}_{CG,polygon}^{\mathbf{p},2D} \quad (24)$$

$$\mathbf{r}^{\mathbf{p},2D''}=\begin{pmatrix}\cos(\pi/2-\varphi_e) & \sin(\pi/2-\varphi_e)\\ -\sin(\pi/2-\varphi_e) & \cos(\pi/2-\varphi_e)\end{pmatrix}\mathbf{r}^{\mathbf{p},2D'}. \quad (25)$$

Here $\mathbf{r}^{\mathbf{p},2D'}$ and $\mathbf{r}^{\mathbf{p},2D''}$ denote translated and rotated polygon coordinates, respectively.

5) Semi-major and semi-minor axes

To calculate the semi-major and semi-minor axes, the confidence of the 2D polygon, $C^{\mathbf{p},2D}$, and the required reporting confidence of the ellipsoid, $C_{ellipsoid}^{\mathbf{p},3D}$, must be related. Assuming independence between coordinates, it holds that

$$\begin{aligned}C_{ellipsoid}^{\mathbf{p},3D}&=\left(C_{ellipsoid}^{\mathbf{p},3D}\right)^{\frac{1}{3}}\left(C_{ellipsoid}^{\mathbf{p},3D}\right)^{\frac{1}{3}}\left(C_{ellipsoid}^{\mathbf{p},3D}\right)^{\frac{1}{3}}\\ &=\left(C_{ellipsoid}^{\mathbf{p},3D}\right)^{\frac{2}{3}}\left(C_{ellipsoid}^{\mathbf{p},3D}\right)^{\frac{1}{3}}\equiv C_e^{\mathbf{p},2D}C_{altitude}^{\mathbf{p},1D},\end{aligned} \quad (26)$$

where $C_e^{\mathbf{p},2D}$ is the required 2D confidence of the ellipse generating the ellipsoid. Since all distributions are uniform, the following constraint holds for the areas of the polygon, $A^{\mathbf{p},2D}$, and the ellipse, $A_e^{\mathbf{p},2D}$,

$$A_e^{\mathbf{p},2D}=\frac{C_e^{\mathbf{p},2D}}{C^{\mathbf{p},2D}}A^{\mathbf{p},2D}. \quad (27)$$

Using that the area of an ellipse is πab, where a and b denote the semi-major and semi-minor axis, it follows that

$$ab=\frac{1}{\pi}\frac{C_e^{\mathbf{p},2D}}{C^{\mathbf{p},2D}}A^{\mathbf{p},2D}. \quad (28)$$

The algorithm now determines the semi-minor axis that provides the best fit according to the criterion

$$V(b)=\frac{1}{N^{\mathbf{p}}}\sum_{i=1}^{N^{\mathbf{p}}}\left(\left(y_i^{\mathbf{p}''}\right)^2-\left(y_{\mathbf{e}}\left(b,x_i^{\mathbf{p}''}\right)\right)^2\right)^2. \quad (29)$$

Note that *the square* of the y-coordinates of the polygon and the ellipse model is used in the criterion. This avoids the need for separate treatment of the branches of the ellipse curve. The ellipse model $y_{\mathbf{e}}\left(b,x_i^{\mathbf{p}''}\right)$ follows from

$$\frac{x_e^2}{a^2}+\frac{y_e^2}{b^2}=1\cdot \quad (30)$$

When back-substituted in (29), the optimization problem is

$$\begin{aligned}b_e=\Bigg(\arg\min_{b^2}\frac{1}{N^{\mathbf{p}}}\sum_{i=1}^{N^{\mathbf{p}}}\Bigg(&\left(y_i^{\mathbf{p}''}\right)^2-\left(b^2\right)^2\\ &+\left(b^2\right)^2\frac{\pi^2\left(C^{\mathbf{p},2D}\right)^2}{\left(C_e^{\mathbf{p},2D}\right)^2\left(A^{\mathbf{p},2D}\right)^2}\left(x_i^{\mathbf{p}''}\right)^2\Bigg)^2\Bigg)^{\frac{1}{2}},\end{aligned} \quad (31)$$

after elimination of a using (28). A differentiation of the sum of squares, *with respect to* b^2, renders the following cubic equation for b_e^2 from which b_e^2 can be solved

$$\varepsilon_0+\varepsilon_1 b_e^2+\varepsilon_2\left(b_e^2\right)^2+\varepsilon_3\left(b_e^2\right)^3=0 \quad (32)$$

$$\varepsilon_0=-\sum_{i=1}^{N^{\mathbf{p}}}\left(y_i^{\mathbf{p}''}\right)^2 \quad (33)$$

$$\varepsilon_1=\sum_{i=1}^{N^{\mathbf{p}}}\left(1+2\frac{\pi^2\left(C^{\mathbf{p},2D}\right)^2}{\left(C_{\mathbf{e}}^{\mathbf{p},2D}\right)^2\left(A^{\mathbf{p},2D}\right)^2}\left(x_i^{\mathbf{p}''}\right)^2\left(y_i^{\mathbf{p}''}\right)^2\right) \quad (34)$$

$$\varepsilon_2=-\sum_{i=1}^{N^{\mathbf{p}}}3\frac{\pi^2\left(C^{\mathbf{p},2}\right)^2}{\left(C_{\mathbf{e}}^{\mathbf{p},2D}\right)^2\left(A^{\mathbf{p},2D}\right)^2}\left(x_i^{\mathbf{p}''}\right)^2 \quad (35)$$

$$\varepsilon_3=\sum_{i=1}^{N^{\mathbf{p}}}2\frac{\pi^4\left(C^{\mathbf{p},2D}\right)^4}{\left(C_{\mathbf{e}}^{\mathbf{p},2D}\right)^4\left(A^{\mathbf{p},2D}\right)^4}\left(x_i^{\mathbf{p}}\right)^4\cdot \quad (36)$$

The cubic equation can be solved analytically using the techniques of Thomas Harriot [20], then a_e follows from (28).

D. Vertical processing

1) Altitude of ellipsoid center

The exact computation of the vertical center of gravity of the 3D polygon would require integration over the surface. Here a more straightforward approach is taken. This exploits the 2D center of gravity calculation of (17) and (18), applied to z and x (giving $z_{CG}^{\mathbf{p},zx}$), and to z and y (giving $z_{CG}^{\mathbf{p},zy}$), rather than to x and y. The two results are then averaged to get the center point of the ellipsoid as

$$\mathbf{r}_{ellipsoid}^{\mathbf{p}}=\left(\left(\mathbf{r}_{CG,polygon}^{\mathbf{p},2D}\right)^T\quad\left(z_{CG}^{\mathbf{p},zx}+z_{CG}^{\mathbf{p},zy}\right)/2\right)^T. \quad (37)$$

2) Vertical axis of ellipsoid

Since the underlying probability distribution is uniform, it is noted that it is the systematic altitude variation between the polygon corners that matters. Unfortunately the ellipsoid reporting format of [17] does not include a parameter that tilts the ellipsoid with respect to the vertical. This means that the vertical uncertainty of the 3GPP ellipsoid needs to cover the full vertical variation of the 3D polygon that would occur e.g. on a hillside, rather than the orthogonal variation from the mean 3D plane of the polygon. Furthermore, the maximal vertical extension of the 3GPP ellipsoid unfortunately occurs at the center point, rather than at the edges.

The 3GPP ellipsoid point with altitude and uncertainty ellipsoid is still the best available alternative for reporting of altitude in LTE. Since the applied positioning method can be reported to the end user in LTE as the 'Position Data' information element, [9], [10], it is possible to make an interpretation of the reported altitude uncertainty c. This interpretation would be the maximum altitude variation of the 3D-polygon surface rather than a vertical random uncertainty. Since it is geometrically obvious that the maximum and minimum altitude of a 3D-polygon surface occurs in one of the corners, it follows from (14), (26) and the discussion above that a useful estimate of c is

$$c = \frac{1}{2}\left(C^{\mathbf{p},3D}_{ellipsoid}\right)^{\frac{1}{3}}\left(\max_i\left(z_i^{\mathbf{p}}\right) - \min_i\left(z_i^{\mathbf{p}}\right)\right). \qquad (38)$$

V. NUMERICAL RESULTS

A six RBS suburban scenario following the one of [6] was simulated in a hilly region with maximal altitude variations of about 200m/km. CID, TA and RSSs were used for LTE fingerprinting. TA range accuracy was conservatively set to 150 m (1-sigma), cf. [7]. A-GPS high precision positions with an altitude standard deviation of 30 m were simulated. After clustering, fingerprinted polygons with altitude were computed and the transformation to ellipsoid points with altitude and uncertainty ellipsoid was calculated, see Fig. 3. The polygon confidence was 70% and the requested reporting confidence was 95%. Note that Fig. 3 does not show a 3D ellipsoid region, rather a 3D ellipsoid cylinder, together with

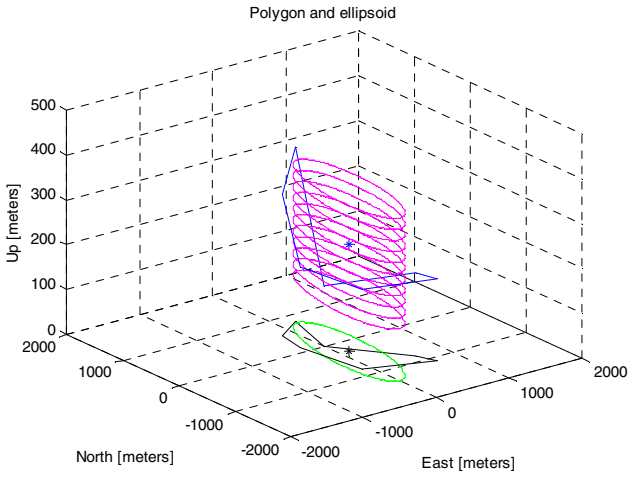

Fig. 3. 3D polygon (blue), ellipsoid cylinder (magenta), and the projection on the horizontal plane, 2D polygon (black) and 2D ellipse (green).

the 3D polygon. The ellipsoid cylinder is the region defined by (38) and the interpretation discussed in section V.D.2.

VI. CONCLUSIONS

The AECID fingerprinting method for the LTE cellular system was extended to a 3D method. A new transformation of the AECID polygon augmented with altitude, to the 3GPP reporting format ellipsoid point with altitude and uncertainty ellipsoid was therefore derived. This enhances E-911 accuracy in metropolitan areas. It is also useful in mountainous regions, where cell phones without A-GPS support that are used e.g. for recreational purposes are provided with an altimeter.

ACKNOWLEDGMENT

The author thanks Erik Schön for the permission to publish.

REFERENCES

[1] The FCC, "Fact sheet – FCC wireless 911 requirements", *FCC,* U.S.A., January, 2001.

[2] S. A. Zekavat and R. M. Buehrer (eds.), *Handbook of Position Location: Theory, Practice and Advances*. Hoboken, NJ: Wiley, 2012.

[3] E. D. Kaplan, *Understanding GPS Principles and Applications.* Norwood, MA: Artech House, 1996.

[4] A. Kangas and T. Wigren, "Location coverage and sensitivity with A-GPS", *URSI Int. Symposium on Electromagnetic Theory*, Pisa, Italy, May 23-27, 2004. Invited paper.

[5] J. F. Bull. "Wireless geolocation - advantages and disadvantages of the two basic approaches for E-911, *IEEE Veh.. Tech. Mag.*, vol. 4, no. 4, pp. 45-53, 2009.

[6] T. Wigren, "Fingerprinting localization using RTT and TA, *IET Comm.* , vol. 6, no. 4, pp. 419-427, 2012.

[7] J. Wennervirta and T. Wigren, "RTT Positioning field performance", *IEEE Trans. Veh. Tech.*, vol. 59, no. 7, pp. 3656-3661, 2010.

[8] A. Kangas and T. Wigren, " Low cost AoA localization in LTE using MIMO precoder index feedback", *submitted to IEEE PIMRC 2012*, 2012.

[9] *Evolved Universal Terrestrial Radio Access (E-UTRA): LTE Positioning Protocol (LPP),* 3GPP TS 36.355, rev. 9.0.0, 2010. Available http://www.3gpp.org/ftp/Specs/html-info/36355.htm.

[10] *Evolved Universal Terrestrial Radio Access (E-UTRA): LTE Positioning Protocol A (LPPa),* 3GPP TS 36.455, rev. 9.0.0, 2010. Available http://www.3gpp.org/ftp/Specs/html-info/36455.htm.

[11] M. I. Simic and P. V. Pejovic, "An algorithm for determining mobile station location based on space segmentation", *IEEE Comm. Letters,* vol. 12, no. 7, pp. 499-501, 2008.

[12] S.-H. Fang, Y.-T. Hsu and W.-H. Kuo, "Dynamic fingerprinting combination for improved mobile localization", *IEEE Trans. Wireless Comm.,* vol. 10, no. 12, pp. 4018-4022, 2011.

[13] M. Ibrahim and M. Youssef, "An energy-efficient GSM positioning system", *IEEE Trans. Veh. Tech.*, vol. 61, no. 1, pp. 286-296, 2012.

[14] L. Shi and T. Wigren, "AECID fingerprinting positioning performance", *in Proc. Globecomm 2009,* Honolulu, Hawaii, dec. 2009.

[15] T. Wigren, "Adaptive enhanced cell-ID fingerprinting localization by clustering of precise position measurements", *IEEE Trans. Veh. Tech.,* vol 56, No. 5, pp. 3199-3209, 2007.

[16] T. Wigren, "Clustering and polygon merging algorithms for fingerprinting positioning in LTE", *in Proc. 5th International conference on signal processing and communication systems, ICSPCS 2011*, Honolulu, HI, December 12-14, 2011.

[17] *Universal Geographical Area Description (GAD),* 3GPP TS 23.032, release 6 (v6.0.0), December, 2004. Available: http://www.3gpp.org/ftp/Specs/html-info/23032.htm.

[18] T. Söderström and P. Stoica, *System Identification.* Hemel Hempstead, UK: Prentice Hall, 1989.

[19] T. Wigren, "A polygon to ellipse transformation enabling fingerprinting and emergency localization in GSM", *IEEE Trans. Veh. Tech.,* vol. 60, no. 4, pp. 1971-1976, 2011.

[20] T. Harriot. *Artes Analyticae Praxis,* 1631.